Available online at www.sciencedirect.com
ScienceDirect
Trans. Nonferrous Met. Soc. China 34(2024) 2354−2366
Transactions of Nonferrous Metals Society of China
www.tnmsc.cn

A short process for organics removal from sodium aluminate solution by regulating electrical double layer of tricalcium aluminate hexahydrate

Zhen-jiang FU[1], Gui-hua LIU[1], Tian-gui QI[1], Lei-ting SHEN[1], Zhi-hong PENG[1], Qiu-sheng ZHOU[1], Yi-lin WANG[1], Hui FANG[2], Yong-lin WANG[2]

1. School of Metallurgy and Environment, Central South University, Changsha 410083, China;
2. Longkou Donghai Alumina Company Limited, Longkou 265713, China

Received 15 January 2023; accepted 3 July 2023

Abstract: The economical removal of organics from sodium aluminate solutions has been required for decades. Based on security filtration using tricalcium aluminate hexahydrate (TCA) as a filter aid, a novel short process to eliminate impurity particles and remove organics simultaneously was presented. Ultrafine TCA samples with poor crystallization, high TCA content, high surface free energy, and large lattice distortion were prepared in the concentrated sodium aluminate solution. The zeta potential of the TCA binary mixture in alkaline solutions was linearly depended on the TCA content, suggesting the additivity of the zeta potential in the binary mixture. The variation in the electrical double layer of the TCA binary mixture was demonstrated in the alkaline solution. Furthermore, the ultrafine TCA exhibited a high adsorption capacity for organics with long alkyl chains and high relative-molecular-mass. The adsorption capacity of 69.69 mg/g organic carbon for sodium humate was achieved, whereas the digestion at a high temperature remarkably reduced the adsorption capacity of TCA.

Key words: organics removal; tricalcium aluminate hexahydrate; sodium aluminate solution; zeta potential; electrical double layer

1 Introduction

Owing to degradation from cellulose, lignin, and humate in bauxite, nearly 400 types of organics were determined in a sodium aluminate solution (Bayer liquor) [1−4]. The total organic carbon (TOC) concentration may reach up to 40 g/L, with relative molecular masses ranging from tens to hundreds [5,6]. Because these organic compounds generally exist in the form of sodium-bearing salts, organics in the sodium aluminate solution typically act as surfactants [1,7]. Consequently, in addition to a loss in the caustic soda, organics significantly deteriorate clarification, reduce the precipitation rate, produce poor-quality alumina, and generate rich foams [8−10]. The liquor combustion [11], oxidation [12−14], lime caustification [10,15], precipitation [16], and adsorption [17] have been developed to remove these organics. However, attempts to use liquor combustion are largely declined owing to its high energy consumption and production costs. Oxidation is limited by its low efficiency and the formation of sodium oxalate. Lime caustification and precipitation only remove sodium oxalate. Furthermore, the side-stream process required in this method complicates alumina production and increases the production cost. Therefore, an economical method to efficiently remove organics from the sodium aluminate solutions is required.

The removal of organics from the sodium aluminate solutions by adsorption using inexpensive adsorbents (red mud [7], activated alumina [18],

Corresponding author: Gui-hua LIU, Tel: +86-13875846305, Fax: +86-731-88830453, E-mail: liugh303@csu.edu.cn
DOI: 10.1016/S1003-6326(24)66546-5
1003-6326/© 2024 The Nonferrous Metals Society of China. Published by Elsevier Ltd & Science Press
This is an open access article under the CC BY-NC-ND license (http://creativecommons.org/licenses/by-nc-nd/4.0/)

and coal flash) has been extensively studied owing to its easy practical application. However, the low adsorption capacity (<5 mg/g TOC), high regeneration cost and high adsorbent dosage notably restrain its application. Inexpensive adsorbents and simple processes to remove the organics are necessary for economical removal of organics from Bayer liquor. Approximately 1.5 g/L tricalcium aluminate hexahydrate (TCA, $3CaO·Al_2O_3·6H_2O$), acting as a filter aid, was added to a green sodium aluminate solution (overflow) after clarification to further remove suspended ultrafine particles of inorganics in the security filtration of the Bayer process [19−21]. Assuming that TCA acts as an adsorbent as well as a filter aid, it has the potential for use in a novel simple approach to economically remove organics.

To improve the quality of alumina, suspended ultrafine particles such as sodium aluminosilicate hydrate, ferrous hydroxide, and unreacted bauxite were efficiently removed by adding TCA. The effects of the particle size, morphology, and structure of TCA on filtration performance have been studied in detail [19,22,23]. Desilication and iron removal using TCA were reported [24−26]. However, the removal of organics using TCA was scarcely reported. In contrast to studies on the morphology and particle size of TCA acting as a filter aid, the interaction between organics and TCA may be remarkably complex, mainly owing to the complicated interaction between organics with various functional groups and the TCA filter aid containing $3CaO·Al_2O_3·6H_2O$ and $Ca(OH)_2$. Furthermore, the high ionic strength in the sodium aluminate solution with various ions, as well as the binary mixture in TCA samples (TCA and $Ca(OH)_2$), further complicates the formation of the electrical double layer. These issues directly affect the removal efficiency of organics. Accordingly, further investigation of the surface properties and zeta potential of TCA to improve the adsorption capacity of organics in the concentrated sodium aluminate solution is crucial.

Herein, the morphology, structure, and surface properties of TCA were studied, and the variation in zeta potential was discussed in detail. The relationships among the structure, particle size, morphology, content, and zeta potential of TCA were explored. Afterwards, the structure of the electrical double layer of the binary mixture in the sodium aluminate solution was also examined. The effects of TCA samples and the relative molecular mass of the organics on the removal efficiency were also studied. The results benefit to a deep understanding of the electrical double layer of the binary mixture in solutions with high ionic strength and provide a novel short process to remove organics from Bayer liquor.

2 Experimental

2.1 Materials

(1) Sodium aluminate solution containing organics:

A sodium aluminate solution was prepared by dissolving NaOH and $Al(OH)_3$ into redistilled water. Considering the presence of sodium-bearing organics in Bayer liquor, sodium oxalate, sodium benzoate, sodium humate, and sodium stearate were respectively dissolved in the redistilled water and then added to the sodium aluminate solution to receive the sodium aluminate solution containing organics.

(2) Preparation of $Ca(OH)_2$ slurry

Lime (CaO) was first obtained by calcining $Ca(OH)_2$ at 850 °C for 2 h [27]. Following the method to prepare TCA in alumina refineries, calcined lime was added to the redistilled water with a solid content of approximately 130 g/L to obtain $Ca(OH)_2$ slurry.

(3) Preparation of TCA samples

Based on the molar ratio of $n_{CaO}/n_{Al_2O_3}$, the sodium aluminate solution was mixed with the $Ca(OH)_2$ slurry in a 500 mL beaker for 20−100 min at 95 °C by overhead agitation with an electric mixer. Subsequently, the wet TCA samples were subjected to vacuum filtration. The TCA samples were then used to remove the organics by acting as filter aids, while some TCA samples were washed with boiling water and dried at 100 °C for 2 h for characterization.

NaOH, $Al(OH)_3$, $Ca(OH)_2$, organics, and other reagents were of analytical grade (Sinopharm Chemical Reagents Co., Ltd.).

2.2 Methods

2.2.1 Novel short process to remove organics

Without a side-stream process, TCA was also used as an adsorbent to remove organics from the sodium aluminate solution (overflow) after

clarification in the traditional security filtration in the Bayer process. Unlike the filtering cake pumped back to the washing process of the red mud in the traditional process, the filtering cake-adsorbed organics were discharged along with the red mud after washing (Fig. 1). Therefore, the short novel process allows TCA to simultaneously act as a filter aid for eliminating suspended particles and act as adsorbents for organic removal.

The dotted line represents the process where TCA acts as a filter aid, which is traditionally adopted in the Bayer process. The full line stands for the novel process where TCA simultaneously acts as a filter aid and adsorbent. After TCA adsorbed organics, it was pumped into the underflow of the last tank during the red mud washing process. The conventional washing process generally contains four or five tanks to separate red mud from the solution.

2.2.2 Procedure

During the security filtration, 1.5 g/L TCA sample was added to the sodium aluminate solution (ρ_{Na_2Ok}=150 g/L, and α_k=1.45) containing organics at 95 °C and stirred at 100 r/min for 20−100 min. Vacuum filtration was then performed to obtain the TCA residue. The TCA residue was used to determine the organic carbon content.

2.3 Characterization

The X-ray diffraction (XRD) patterns were recorded using an XRD instrument (Rigaku Smart Lab 9 kW) with Cu K_α radiation at a scanning rate of 5 (°)/min. The tube voltage, electric current, and scanning range were 40 kV, 250 mA, and 10°−80°, respectively. The morphology of TCA was determined using scanning electron microscopy (SEM) at an accelerating voltage of 20 kV (JSM−6360LV, JEOL, Japan). Fourier-transform infrared (FTIR) spectroscopy (Nicolet 6700, Thermo Scientific, US) was performed in the range of 400−4000 cm^{-1} at a resolution of 4 cm^{-1} with 32 scans. The particle size distribution (PSD) was determined using a laser particle analyzer (MS 2000, Malvern Instruments, UK). The zeta potential was measured using a zeta-potential analyzer (Zano−zs, Malvern Instruments, UK).

Semi-quantitative analysis of the TCA and $Ca(OH)_2$ phases content was determined by relative intensity ratio (RIR) method according to Eq. (1) [28,29]:

$$X_i = \frac{I_i K_i}{\sum_{j=1}^{n} I_j K_j} \times 100\% \quad (1)$$

where X_i is the mass fraction of phase i in the sample; I_i and I_j are the integrated intensities of the strongest diffraction peak of phase i and j, respectively; K_i and K_j stand for the ratio of $I_i/I_{\alpha\text{-}Al_2O_3}$ and $I_j/I_{\alpha\text{-}Al_2O_3}$, respectively ($\alpha$-$Al_2O_3$ is the reference phase); n is the number of phases in the sample.

The crystallite size (D) and microstrain (ε) for the preferential orientation of TCA and $Ca(OH)_2$ were calculated from the XRD patterns using the Debye−Scherrer equations [30,31]:

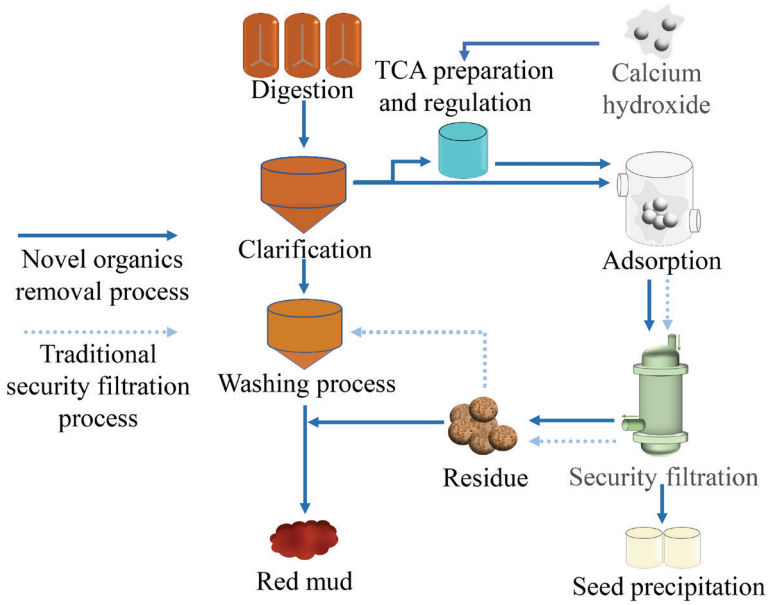

Fig. 1 Novel and traditional process of security filtration in Bayer process

$$D=\frac{K\lambda}{\beta\cos\theta} \tag{2}$$

$$\varepsilon=\frac{\beta}{4\tan\theta} \tag{3}$$

where K and λ are the Scherrer constant and wavelength of the X-ray radiation, respectively; θ is the Bragg angle of the peak and β is the peak at the full width of the sample (FW(S)).

The contact angle was first recorded with a contact angle/surface tension meter (LSA100, LAUDA Scientific, GER) at 298 K. The surface dispersion force (r_s^d), polarity force (r_s^p), and free energy (r_s) were calculated according to Eqs. (4) and (5), using the Owens two-liquid method [32]. The solvation trend was determined by the ratio of the polarity force to the dispersion force (r_s^p/ r_s^d) [33]:

$$\gamma_l(1+\cos\theta')=2(\gamma_s^d\cdot\gamma_l^d)^{1/2}+2(\gamma_s^p\cdot\gamma_l^p)^{1/2} \tag{4}$$

$$\gamma_s=\gamma_s^d+\gamma_s^p \tag{5}$$

where γ_l is the surface tension of water or diiodomethane at 298 K and θ' represents the contact angle. γ_l^d and γ_l^p of water are 21.8 and 51 mJ/m, respectively. γ_l^d and γ_l^p of diiodomethane are 48.5 and 2.3 mJ/m, respectively [34,35].

The organic carbon content of the TCA samples (adsorption capacity, q, mg/g) was determined by titration with potassium dichromate (potassium dichromate external heating method) according to Eq. (6) [36,37]:

$$q=\left[\frac{5c}{V_0}(V_0-V)\times10^{-3}\times3.0\times1.1/m\right]\times100\% \tag{6}$$

where c is 0.8 mol/L, obtained from concentration of 1/6$K_2Cr_2O_7$ standard solution. 5 mL $K_2Cr_2O_7$ was used as standard solution. V_0 and V (mL) are the volumes of the $FeSO_4$ solution consumed in the blank and sample groups, respectively. Further, the universal correction factor of oxidization was taken as 1.1. m (g) is the measured sample mass.

The standard error (σ) in the form of an error bar was calculated using Eq. (7) after repeating the experiments under the same conditions:

$$\sigma=\frac{D_S}{\sqrt{N}} \tag{7}$$

where D_S and N (≥3) are the standard deviation and number of samples, respectively.

3 Results and discussion

3.1 Morphology and particle size of TCA samples

Based on the traditional process of removing inorganic impurities in the form of suspended ultrafine particles, the concentrated sodium aluminate solution (green liquor from overflow) at 95 °C was used to prepare the TCA samples. Figure 2 and Table 1 show SEM images and PSD values of TCA samples prepared under different reaction conditions.

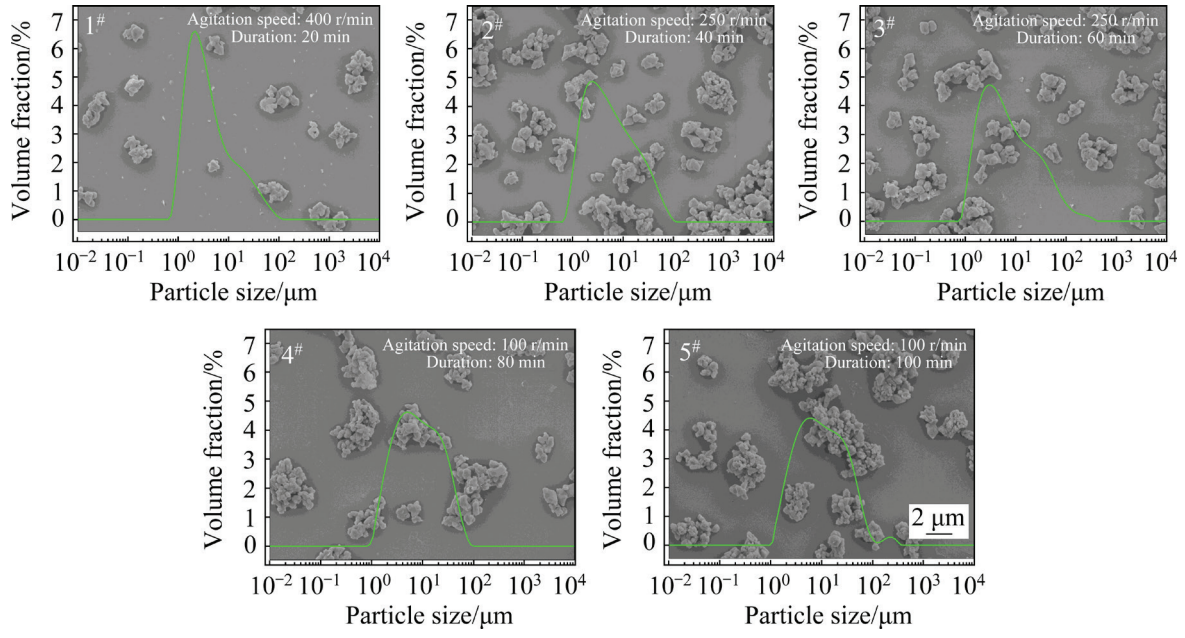

Fig. 2 SEM images and PSD curves of samples under different reaction conditions (T=95 °C; ρ_{Na_2Ok}=150 g/L; α_k=1.45)

Table 1 Particle size of samples under various conditions

Sample	Agitation speed/ ($r \cdot min^{-1}$)	Duration/ min	d_{10}/ μm	d_{50}/ μm	d_{90}/ μm
1#	400	20	1.247	3.061	19.143
2#	250	40	1.381	4.554	25.976
3#	250	60	1.592	5.510	40.116
4#	100	80	2.092	7.525	30.348
5#	100	100	2.311	8.846	38.589

As shown in Fig. 2 and Table 1, a strong agitation with a short duration in the preparation of TCA samples produced the ultrafine TCA particle of Sample 1# with minor particle agglomeration. A prolonged duration and weak agitation (Samples 2# and 3#) enlarged the particle size and promoted the agglomeration of the ultrafine particles, as verified by the widened peak in Fig. 2. Further prolonging the duration and reducing the agitation speed (Samples 4# and 5#) generated coarse TCA particles in a cauliflower shape. This implies that an increase in the agitation speed generates the ultrafine particles of TCA with a relatively high specific surface area, possibly favoring the removal of organics from the sodium aluminate solution.

3.2 Phase composition and surface properties of TCA binary mixture

3.2.1 Phase composition and structure

$Ca(OH)_2$ is difficult to dissolve in the concentrated sodium aluminate solution, suggesting that $Ca(OH)_2$ and TCA coexist after the lime slurry is added to the sodium aluminate solution. Figure 3(a) shows the XRD patterns and distribution of $Ca(OH)_2$ and TCA contents (wt.%) in various TCA samples, and Fig. 3(b) shows the schematic of the TCA composition.

Owing to the high Na_2O concentration, TCA and $Ca(OH)_2$ were both found in TCA samples 1#–5# (also expressed as a TCA binary mixture). Furthermore, weak agitation for a long duration reduced the TCA content but increased the $Ca(OH)_2$ content. This is because the $Ca(OH)_2$ particles are readily enveloped by the ultrafine TCA particles, hindering the further reaction of $Ca(OH)_2$ with $Al(OH)_4^-$ (Fig. 3(b)). Meanwhile, strong agitation for a short duration favored the mass transfer of Ca^{2+} in $Ca(OH)_2$, leading to the shrinking inner core of $Ca(OH)_2$ and an increase in TCA content. Correspondingly, an increase in the volume fraction of TCA particles ranging from 1 to 10 μm (Fig. 2) was observed.

Based on the XRD patterns shown in Fig. 3(a), Table 2 displays the cell volume (V), FWHM, microstrain (ε), and crystallite size (D) of TCA and $Ca(OH)_2$.

The cell volumes (V) of TCA and $Ca(OH)_2$ from TCA samples 1#–5# both gradually approached the cell volume of the standard (1987.54 $Å^3$ in PDF 72-1109, 54.82 $Å^3$ in PDF 76-0571). An increase in the deviation of the cell volumes and FWHM generally increased the microstrain (ε) and lattice distortion. This suggests that the short duration and increasing agitation speed generate more active sites on the surface of Sample 1# compared with Sample 5#.

To further observe the crystallization of TCA prepared under various conditions, FTIR spectra of the TCA samples in the wavenumber range of 3720−3600 cm^{-1} are shown in Fig. 4.

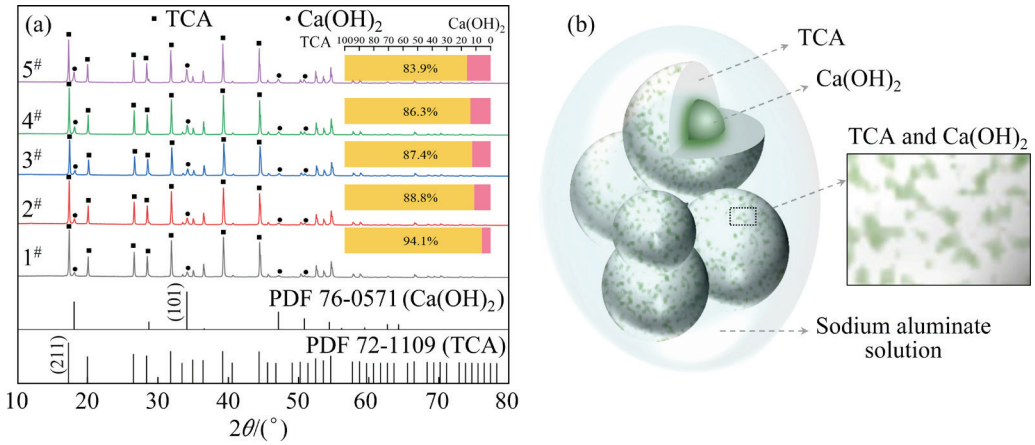

Fig. 3 XRD patterns and TCA content in samples prepared under different reaction conditions (a) and schematic of binary mixture (b)

Table 2 Cell parameters of TCA samples under different reaction conditions

Sample	TCA (211)			$Ca(OH)_2$ (101)			
	V/Å^3	FWHM/(°)	$\varepsilon/10^{-3}$	V/Å^3	FWHM/(°)	D/Å	$\varepsilon/10^{-3}$
1#	1984.48	0.139	2.430	55.01	0.228	498	2.450
2#	1985.35	0.134	2.296	55.03	0.232	486	2.521
3#	1985.48	0.128	2.124	55.01	0.230	492	2.485
4#	1986.70	0.118	1.838	54.98	0.215	538	2.245
5#	1986.13	0.118	1.847	54.95	0.211	551	2.166

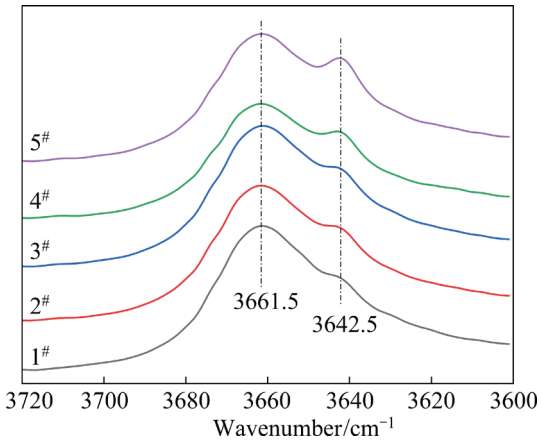

Fig. 4 FTIR spectra of TCA samples

The stretching vibration peak of the free O—H bond at 3661.5 cm^{-1} was assigned to the internal structural hydroxyl of TCA. Another stretching vibration peak for the O—H bond at 3642.5 cm^{-1} was observed for the 1#–5# TCA samples, which was mainly due to the formation of a hydrogen bond (H—O···H) between —OH groups. This proves the existence of a significant microstrain in the structure of Sample 1# but a high level of crystallization in Sample 5# [38,39].

3.2.2 Surface contact angle and surface force of TCA binary mixture

The PSD, morphology, TCA content, and structure of TCA depended on the agitation speed and duration, and the surface properties of the TCA samples changed accordingly. The contact angle, dispersion force (r_s^d), polarity force (r_s^p), and surface free energy (r_s) values are listed in Table 3.

The results in Table 3 show reductions in r_s^d, r_s^p, and r_s from Sample 1# to Sample 5#. This is mainly due to the reduction in the TCA content and a high level of crystallization from Sample 1# to Sample 5#, as shown in Fig. 4.

Compared to the desilication product (DSP), calcium−silicate residue, calcium−titanate, hematite, magnetite in red mud, and gibbsite [33,40,41] in Table 4, the surface of TCA was characterized by a high polarity force (29.17 mN/m), which possibly improved dipole−dipole interactions between the TCA surface and the polar groups of the surfactants. Furthermore, the increase in the ratio of the polarity force to the dispersion force (r_s^p/r_s^d), from 0.61 for Sample 5# to 0.60 for Sample 1# implies a strong interaction between TCA and the organics. Meanwhile, the surface free energy of Sample 1# reached 77.81 mN/m, which was much higher than that of the substances in Table 4. This finding implies that TCA owns good adsorption performance in Bayer liquor.

3.3 Zeta potential of TCA samples in alkaline solutions

Although the zeta potential has been extensively studied for solid−liquid interfaces of single solid samples, the variation in the zeta potential of mixtures has been scarcely reported. The as-synthesized TCA binary mixture exhibited different structures, crystallization, and surface properties. These variations could lead to a variable zeta potential by the preferential adsorption of various ions from Bayer liquor, providing an approach to regulate the removal efficiency of organics. Therefore, the zeta potential of the TCA binary mixture was recorded in the dilute NaOH and the concentrated sodium aluminate solution.

3.3.1 Zeta potential of TCA samples in dilute NaOH solution

Samples 1#–5# were characterized by a positive potential in the pH range of 8−14, as shown in Fig. 5. The zeta potential of Sample 1# was the lowest, while that of Sample 5# was the highest. Meanwhile, an increase in the pH from 8 to 14 led to a notable reduction in the zeta potential of the TCA samples.

Table 3 Average contact angle and surface force of Samples 1#, 3#, and 5#

Sample	Contact angle/(°)		r_s^p/(mN·m^{-1})	r_s^d/(mN·m^{-1})	r_s/(mN·m^{-1})
	Water	Diiodomethane			
1#	17.4	26.2	29.17	48.64	77.81
3#	22.2	29.3	28.47	46.97	75.44
5#	29.4	34.9	26.94	44.21	71.15

Table 4 Physics constants of substances in Bayer liquor

Substance	r_s^p/(mN·m^{-1})	r_s^d/(mN·m^{-1})	r_s/(mN·m^{-1})	r_s^p/r_s^d
DSP	18.87	39.65	56.95	0.50
Hematite	19.38	43.13	59.03	0.49
Magnetite	14.41	40.44	54.85	0.36
Goethite	14.67	40.83	55.50	0.36
Calcium titanate	17.85	39.54	57.39	0.45
Limestone	8.43	43.59	52.02	0.19
Dicalcium silicate	19.07	37.94	57.01	0.50
Aluminum hydroxide	8−9	39−40	≈48	≈0.20

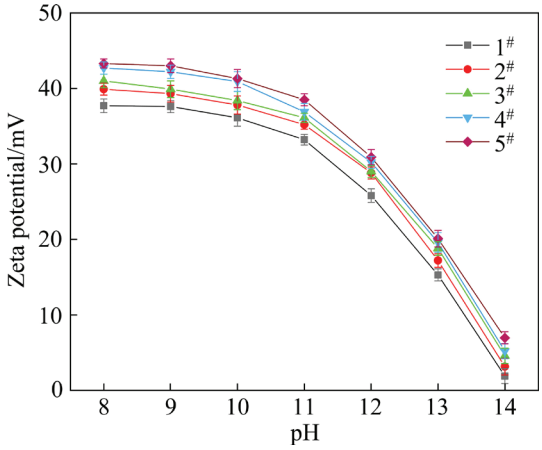

Fig. 5 Effect of pH on zeta potential of TCA in dilute NaOH solution

The positive zeta potential is mainly due to the occurrence of Ca^{2+} from $Ca(OH)_2$ and TCA according to Eqs. (8)−(10) [21,42]:

$$3CaO{\cdot}Al_2O_3{\cdot}6H_2O \rightleftharpoons 3Ca^{2+}+2Al(OH)_4^-+4OH^- \quad (8)$$

$$3CaO{\cdot}Al_2O_3{\cdot}6H_2O+2NaOH \rightleftharpoons 3Ca(OH)_2+2NaAl(OH)_4 \quad (9)$$

$$Ca(OH)_2 \rightleftharpoons Ca^{2+}+2OH^- \quad (10)$$

TCA and $Ca(OH)_2$ in the TCA binary mixture both provide Ca^{2+}, and Ca^{2+} preferentially constitutes the electrical double layer and contributes to the positive charges of the particles. An increase in the pH increases the stability of $Ca(OH)_2$, and the migration of OH^- to the electrical double layer reduces the zeta potential. Meanwhile, because $Ca(OH)_2$ is less stable than TCA [20,21], the increase in the $Ca(OH)_2$ content in Sample 5# increases the zeta potential. However, the poor crystallization, strong polar surface, and high surface free energy of Sample 1# may promote the adsorption of anions in the electrical double layer, leading to the lowest zeta potential.

3.3.2 Zeta potential of TCA samples in sodium aluminate solution

TCA, which acts as a filter aid, is generated in the concentrated sodium aluminate solution. The zeta potentials of Samples 1#−5# in the sodium aluminate solution (ρ_{Na_2Ok}=30.7 g/L, and α_k=3.0) are plotted in Fig. 6(a).

In contrast to the positive potential in the dilute NaOH solution (8 < pH < 14), the zeta potentials of Samples 1#−5# were all negative in the sodium aluminate solution. The phenomena are mainly caused by $Al(OH)_4^-$ in the sodium aluminate solution, which readily enters the electrical double layer [43]. Meanwhile, the substantial adsorption capacity of Sample 1# for $Al(OH)_4^-$ and OH^- led to the most negative zeta potential, whereas Sample 5#, with the highest content of $Ca(OH)_2$ and a high level of crystallization, was characterized by the highest zeta potential.

Based on the contents of TCA and $Ca(OH)_2$ in the TCA binary mixture, the line relationships between the TCA content (C_{TCA}) and zeta potential (ζ) in alkaline solutions are shown in Fig. 6(b) and Table 5. An increase in pH results in a decrease in the absolute value of the slope, indicating that the electrical double layer is more stable resulting from the adsorption of $Al(OH)_4^-$ and OH^- in the alkaline solution. The linear relationships (Eqs. (11) and (12)) in the sodium aluminate solution for the binary mixture (TCA and $Ca(OH)_2$) imply the occurrence of composition additivity for the zeta

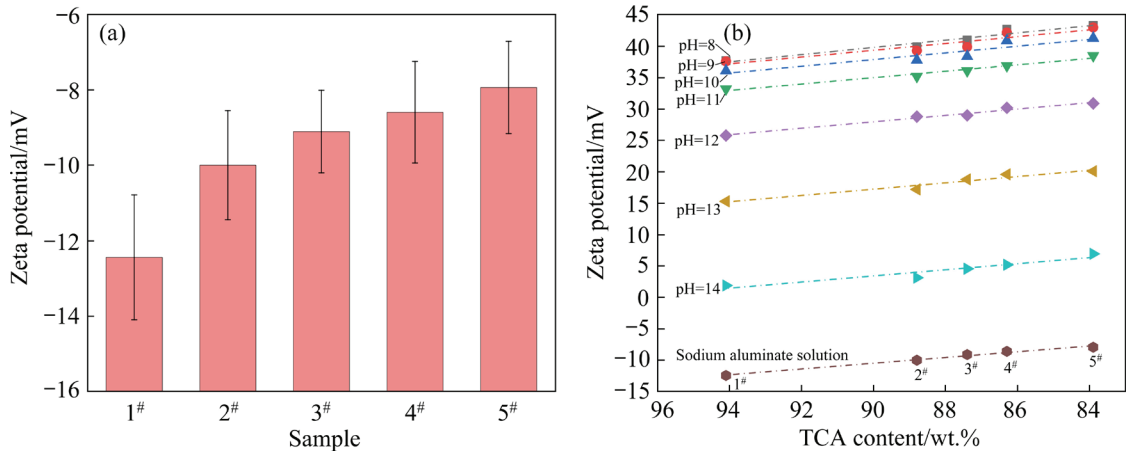

Fig. 6 Zeta potentials of Samples 1#–5# in sodium aluminate solution (a) and effect of TCA content on zeta potential in alkaline solutions (b) (ρ_{Na_2Ok}=30.7 g/L; α_k=3.0)

Table 5 Intercept, slope, and R^2 of fitting equations in Fig. 6(b)

Data	pH=8	pH=9	pH=10	pH=11	pH=12	pH=13	pH=14	Sodium aluminate solution
Intercept	91.61±7.00	88.18±10.11	85.95±10.70	80.97±4.52	73.8 ±3.61	62.39±5.93	47.19±7.63	30.63±2.52
Slope	−57.54±7.94	−54.23±11.46	−53.40±12.14	−51.07±5.13	−50.95±4.10	−50.16±6.72	−48.62±8.66	−45.69±2.86
R^2	0.93	0.84	0.82	0.96	0.97	0.93	0.88	0.98

potential. These findings suggest that the zeta potential of TCA can be quantitatively regulated based on the distributions of TCA and $Ca(OH)_2$. Furthermore, according to Eqs. (11) and (12), the TCA phase was characterized by a negative zeta potential, and $Ca(OH)_2$ owned a positive zeta potential from the positive intercepts in the sodium aluminate solution, owing to $Al(OH)_4^-$ entering the electrical double layer preferentially (specific adsorption) of TCA.

$$\zeta=30.63-45.69C_{TCA} \quad (11)$$

$$\zeta=-15.06+45.69C_{Ca(OH)_2} \quad (12)$$

3.3.3 Zeta potential of TCA samples in sodium aluminate solution containing organics

Sodium-bearing organics in the concentrated sodium aluminate solution predominantly exist in the form of anionic surfactants [1,44]. These surfactants may be preferentially adsorbed on the surface of TCA through electrostatic forces and specific adsorption. The effects of the organics on the zeta potential of TCA are listed in Table 6.

Based on the zeta potential of Sample 3# (−8.62 mV) in the sodium aluminate solution without organics, the organics in sodium aluminate solution notably reduced the zeta potential of TCA. Surfactants with long alkyl chains (SM and SS) further reduced the zeta potential, mainly owing to the ideal surface activity and specific adsorption through the strong interaction between the surfactant and particle surface [45,46]. For example,

Table 6 Effects of organics on zeta potential of Sample 3# in sodium aluminate solution

Organic	Molecular formula	Content/ 10^{-6}	Zeta potential/mV
Blank	–	–	−8.62
Sodium oxalate (SO)	$Na_2C_2O_4$	110	−10.54
Sodium benzoate (SB)	$C_7H_5NaO_2$	104	−15.23
Sodium dodecyl sulfate (SDS)	$C_{12}H_{25}SO_4Na$	104	−29.80
Sodium myristate (SM)	$C_{14}H_{27}NaO_2$	102	−34.22
Sodium stearate (SS)	$C_{18}H_{35}NaO_2$	104	−36.90
Sodium humate (SH)	–	52	−22.60

TCA content: ~1.5 g/L, ρ_{Na_2Ok}=30.7 g/L, α_k=3.0

compared with sodium oxalate, stearate ions were preferentially adsorbed on the TCA surface, further reducing the zeta potential.

3.3.4 Effect of electrical double layer on zeta potential of TCA samples in alkaline solution

Based on the variation in the zeta potential of TCA in the dilute NaOH solution, sodium aluminate solution, and sodium aluminate solution containing organics, a schematic diagram of the electrical double layer of the TCA binary mixture is shown in Fig. 7.

TCA and $Ca(OH)_2$ are both nearly insoluble, and the presence of OH^- in the alkaline solution further reduces their solubility. The high Ca^{2+} content provided by $Ca(OH)_2$ and TCA in the dilute NaOH solution was present in the electrical double layer, leading to a positive zeta potential (Fig. 7(a)). Due to electrostatic forces and specific adsorption, $Al(OH)_4^-$ readily entered the inner Helmholtz plane (IHP) of TCA particles, leading to different structures of the Stern double layer. A few cations were attracted by anions gathered in IHP and the outer Helmholtz plane (OHP) was formed [47,48]. Meanwhile, more $Al(OH)_4^-$ was present in the electrical double layer, which further reduced the zeta potential (Fig. 7(b)). In addition to OH^- and $Al(OH)_4^-$, organic anions in the sodium aluminate solution preferentially entered the IHP through specific adsorption and electrostatic forces. The anions present in the electrical double layer further reduced the zeta potential (Fig. 7(c)). Based on the zeta potential, the preferential occurrence of anions in the electrical double layer followed the order of organic anion > $Al(OH)_4^-$ > OH^- in the alkaline solution. Furthermore, the relatively less stable $Ca(OH)_2$ in the TCA binary mixture provided some Ca^{2+} in the electrical double layer, increasing the zeta potential in the TCA binary mixture.

In summary, because of the variable phase composition, TCA structure, surface energy, and anions in the sodium aluminate solution, the zeta potential was reduced from the dilute NaOH solution to the sodium aluminate solution. The preferential migration of organic anions into the electrical double layer further changed the electrical double layer and decreased the zeta potential. Compared to DSP, calcium−silicate residue, calcium−titanate, and hematite in red mud with low surface energy [33,40,41], TCA may be a more promising adsorbent for economically removing organics from sodium aluminate solutions by regulating the TCA purity, structure, and surface properties.

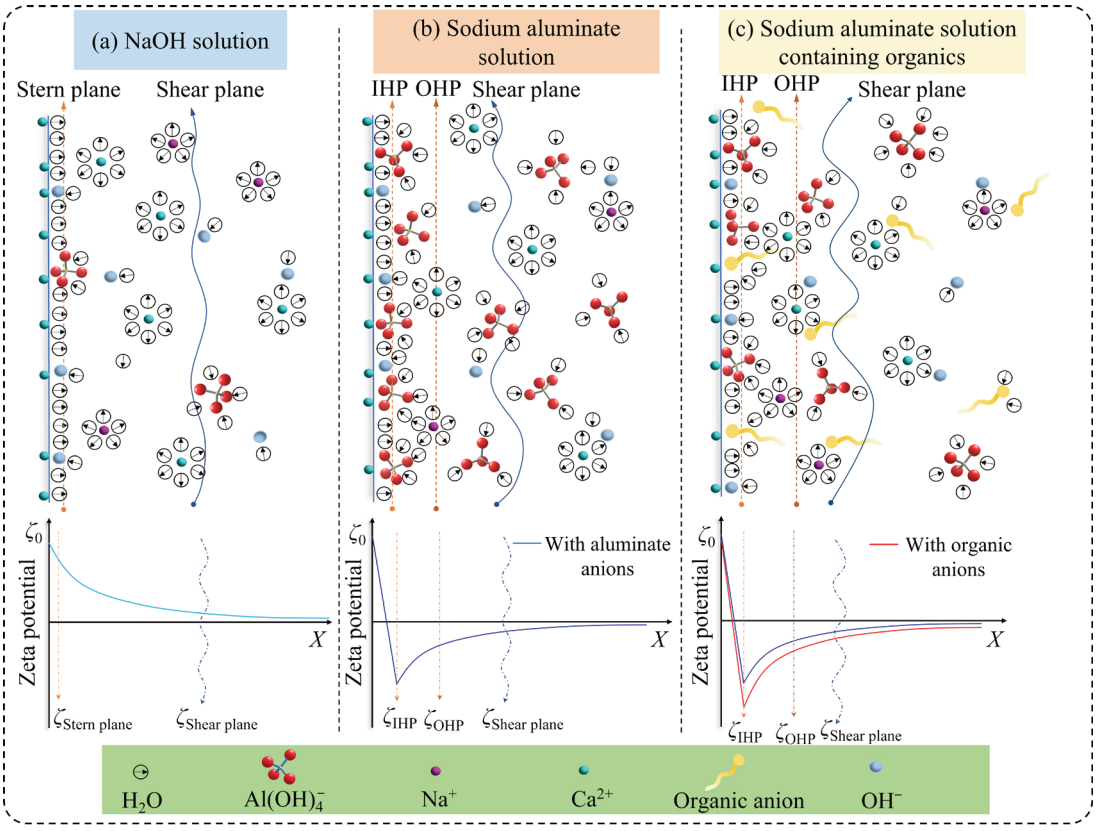

Fig. 7 Schematic diagram and potential trend of electrical double layer with TCA present in alkaline solution

3.4 Economical removal of organics with TCA in sodium aluminate solution

3.4.1 Effect of organics on adsorption capacity of TCA binary mixture

A notable reduction in the zeta potential implies that organics removal with TCA is feasible. Therefore, the adsorption capacities of Samples 1#−5# in the concentrated sodium aluminate solution containing various organics are presented in Fig. 8.

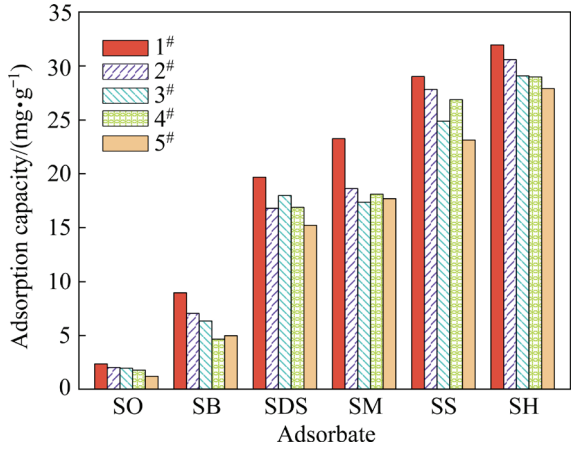

Fig. 8 Effect of organics on adsorption capacities of TCA samples (ρ_{Na_2Ok}=150 g/L; α_k=1.45; organics concentration: 0.5 g/L; T=95 °C; t=60 min; agitation speed: 100 r/m; TCA content: 1.5 g/L)

As shown in Fig. 8, the adsorption capacity was high for organics with long alkyl chain and high relative-molecular-mass (SS and SH), while it was less than 8 mg/g for SO and SB. This is in good agreement with the zeta potentials of the TCA samples (Table 6). Owing to the longer chain of SS compared to SM, SS can readily self-assemble into micelles [49]. Furthermore, increasing the concentration of the organics (0.5 g/L in Fig. 8) benefited to multilayer adsorption at the TCA interfaces [50]. Therefore, the adsorption capacity of TCA for SS was significantly increased. In addition, the adsorption capacities of Sample 1# reached 31.95 and 29.01 mg/g in the solutions containing SH and SS, respectively, much higher than those of active alumina and red mud [7,18]. This finding suggests that TCA can efficiently remove organics with medium and high relative-molecular-mass from Bayer liquor.

The results in Fig. 8 also show that the highest adsorption capacity for organics was obtained with Sample 1# compared to other TCA samples in solution containing organics with various relative-molecular-mass. This suggests that ultrafine particle, weak agglomeration, large lattice distortion, strong polar surface, high surface free energy, good solvation trend (r_s^p/r_s^d), high content of TCA, and small zeta potential are conducive to the efficient removal of organics in the sodium aluminate solution.

3.4.2 Effect of digestion on SH removal with TCA

The humic acid in bauxite is readily dissolved in the sodium aluminate solution in the form of sodium humate (SH). SH is consequently degraded into various organics in the sodium aluminate solution at high temperatures. According to the digestion temperatures of gibbsite and diasporic bauxite (145 and 280 °C, respectively), the effect of the digestion temperature on the adsorption capacity of TCA is shown in Fig. 9.

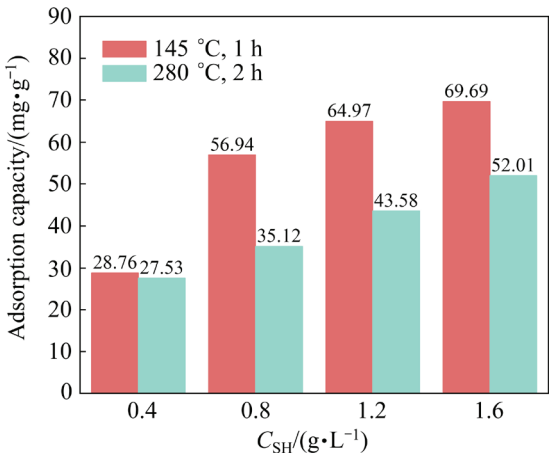

Fig. 9 Effect of different digestion conditions and SH concentration (C_{SH}) on adsorption capacity of Sample 1# (ρ_{Na_2Ok}=150 g/L; α_k=1.45; T=95 °C; t=60 min; agitation speed: 100 r/m; TCA content: ~1.5 g/L)

The results in Fig. 9 show that increasing the SH concentration increased the adsorption capacity of TCA. In particular, a significant increase in the adsorption capacity was observed from 0.4 to 0.8 g/L, and a slight increase in the adsorption capacity was found with a further increase in the SH concentration, possibly owing to the micellar adsorption increasing the repulsive forces among OH^-, $Al(OH)_4^-$, and single organic anions [2,49]. The maximum removal of 69.69 mg/g organic carbon was achieved at 1.6 g/L SH after digestion at 145 °C for 1 h. Meanwhile, the adsorption capacity was notably reduced for SH digested at 280 °C owing to the decomposition of SH in the concentrated alkaline solution at a high temperature.

This is consistent with the low adsorption capacity of organics with short alkyl chains, as shown in Fig. 8. Correspondingly, the dark black sodium aluminate solution changed into a gray–orange solution (Fig. 10) after the removal of organics. These results prove that organics removal from a sodium aluminate solution is a promising method, where TCA simultaneously acts as an adsorbent and filter aid. Further studies on the electrical double-layer structure of the mixture and increasing the adsorption capacity should be carried out.

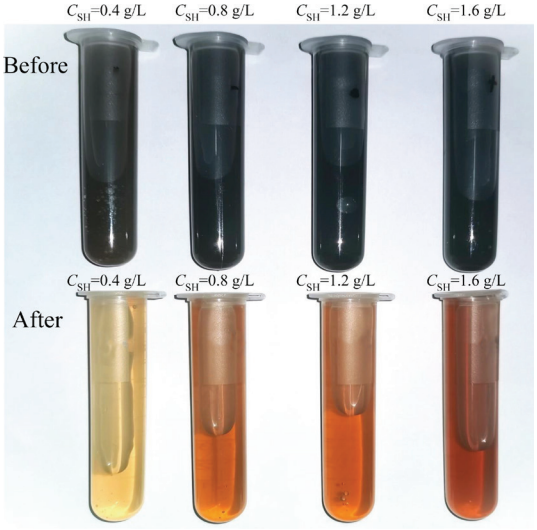

Fig. 10 Comparison of solution color before and after adsorption (Digestion temperature: 145 °C; digestion time: 1 h; TCA content: ~1.5 g/L)

4 Conclusions

(1) TCA prepared from an aluminate solution was present in the binary mixture. Shortening the duration and increasing the agitation speed generated ultrafine TCA samples with poor crystallization, high TCA content, high surface free energy, large lattice distortion, and large microstrain.

(2) Increasing the pH from 8 to 14 notably reduced the zeta potential in the dilute NaOH solution. The preferential adsorption of $Al(OH)_4^-$ gave rise to a negative zeta potential in the sodium aluminate solution. Anionic organics with long alkyl chains and high relative-molecular-mass further reduced the zeta potential. Ultrafine TCA with poor crystallization was characterized by a further negative zeta potential. Furthermore, the zeta potential was linearly depended on the TCA content in TCA samples, suggesting the additivity of the zeta potential in the binary mixture.

(3) Ultrafine TCA with poor crystallization and anionic organics with long alkyl chains and high relative-molecular-mass both increased the adsorption capacity of TCA. The digestion of SH at high temperatures reduced the adsorption capacity of TCA. An adsorption capacity of 69.69 mg/g was achieved for SH, accompanied by a change in the solution color from black to gray–orange.

CRediT authorship contribution statement

Zhen-jiang FU: Methodology, Data curation, Writing – Original draft, Preparation; **Gui-hua LIU:** Funding acquisition, Supervision, Conceptualization, Writing – Review & editing; **Tian-gui QI:** Methodology, Data curation; **Lei-ting SHEN:** Writing – Review & editing, Supervision; **Zhi-hong PENG:** Investigation, Writing – Review & editing; **Qiu-sheng ZHOU:** Methodology, Writing – Review & editing; **Yi-lin WANG:** Data curation, Writing – Review & editing, Supervision; **Hui FANG:** Resources; **Yong-lin WANG:** Resources, Project administration.

Declaration of competing interest

The authors declare that they have no known competing financial interests or personal relationships that could have appeared to influence the work reported in this paper.

Acknowledgments

The authors gratefully appreciate the financial support provided by the National Natural Science Foundation of China (No. 51874366).

References

[1] FRANCESCO B, LYNDON B, SUZANNE M, ANNA H, ANN J C, JOANNE L, GREG P. Physicochemical characterization of organic matter in Bayer liquor [J]. Industrial & Engineering Chemistry Research, 2014, 53(15): 6544−6553.

[2] WU Peng, LIU Gui-hua, LI Xiao-bin, PENG Zhi-hong, ZHOU Qiu-sheng, QI Tian-gui, WANG Yi-lin, SHEN Lei-ting, FANG Hui, WANG Yong-lin. Multilayer adsorption improving the organic removal by foam flotation from sodium aluminate solutions [J]. Colloids and Surfaces A: Physicochemical and Engineering Aspects, 2022, 654: 130126.

[3] MACHOLD T, LAIRD D W, ROWEN C C, MAY P M, HEFTER G T. Decomposition of Bayer process organics: Phenolates, polyalcohols, and additional carboxylates [J]. Hydrometallurgy, 2011, 107(3): 68−73.

[4] ZHANG Ye, XU Rui, TANG Hong-hu, WANG Li, SUN Wei. A review on approaches for hazardous organics removal

from Bayer liquors [J]. Journal of Hazardous Materials, 2020, 397: 122772.

[5] GREG P, JOANNE S C L, JOHANNES E W, FRANCESCO B, CYNTHIA J. A review of the determination of organic compounds in Bayer process liquors [J]. Analytica Chimica Acta, 2011, 689(1): 8−21.

[6] GREG P, JOANNE S C L, KLAUS N. Organic compounds in the processing of lateritic bauxites to alumina: Part 1. Origins and chemistry of organics in the Bayer process [J]. Hydrometallurgy, 2010, 105(1): 1−29.

[7] WU Peng, LIU Gui-hua, LI Xiao-bin, PENG Zhi-hong, ZHOU Qiu-sheng, QI Tian-gui. Effects of CMC and micelle formation on the removal of sodium benzoate or sodium stearate in a sodium aluminate solution [J]. JOM, 2020, 72(1): 263−269.

[8] SONTHALIA R, BEHARA P, KUMARESAN T, THAKRE S. Review on alumina trihydrate precipitation mechanisms and effect of Bayer impurities on hydrate particle growth rate [J]. International Journal of Mineral Processing, 2013, 125: 137−148.

[9] SMEULDERS D E, WILSON M A, PATNEY H, ARMSTRONG L. Structure of molecular weight fractions of Bayer Humic substances: 2. Pyrolysis behavior of high-temperature products [J]. Industrial & Engineering Chemistry Research, 2000, 39(10): 3631−3639.

[10] ZHANG Bai-yong, PAN Xiao-lin, WANG Jiang-zhou, YU Hai-yan, TU Gan-feng. Reaction kinetics and mechanism of calcium oxide in dilute sodium aluminate solution with oxalate based on lime causticization [J]. Transactions of Nonferrous Metals Society of China, 2019, 29(6): 1312−1322.

[11] WELLINGTON M A. Effect of thermal treatment of bauxite ore on carbon (organic and inorganic) content and solubility in Bayer process liquor [J]. Industrial & Engineering Chemistry Research, 2013, 52(4): 1434−1438.

[12] LI Meng-nan, LIU Zhan-wei, YAN Heng-wei, WEI Jie, LIU Shu-xin. Removal of organic compounds from Bayer liquor by oxidation with sodium nitrate [J]. Hydrometallurgy, 2022: 105972.

[13] SOPLIN M A, BOTELHO JUNIOR A B, BALTAZAR M P G, TENORIO J A S, ESPINOSA D C R. Application of advanced oxidative process for organic compounds removal from Bayer liquor [C]//TOMESETT A. Light Metals 2020. Cham: TMS, 2020: 60−64.

[14] RAN Jian-feng, DUAN Hai-sheng, SRINIVASAKANNAN C, YAO Jia-shu, YIN Shao-hua, ZHANG Li-bo. Effective removal of organics from Bayer liquor through combined sonolysis and ozonation: Kinetics and mechanism [J]. Ultrasonics Sonochemistry, 2022, 88: 106106.

[15] LIU Gui-hua, DONG Wen-bo, QI Tian-gui, ZHOU Qiu-sheng, PENG Zhi-hong, LI Xiao-bin. Behavior of calcium oxalate in sodium aluminate solutions [J]. Transactions of Nonferrous Metals Society of China, 2017, 27(8): 1878−1887.

[16] MAHMOUDIAN M, GHAEMI A, SHAHHOSSEINI S. Removal of carbonate and oxalate pollutants in the Bayer process using thermal and chemical techniques [J]. Hydrometallurgy, 2015, 154: 137−148.

[17] YU Hai-yan, PAN Xiao-lin, DING Ting-ting, ZHANG Wu, LIU Han, BI Shi-wen. Adsorption of sodium polyacrylate at interface of dicalcium silicate–sodium aluminate solution [J]. Transactions of Nonferrous Metals Society of China, 2011, 21(10): 2323−2326.

[18] LIU Gui-hua, CHEN Bin-bin, QI Tian-gui, ZHOU Qiu-sheng, PENG Zhi-hong, LI Xiao-bin, DONG Wen-bo. Removal of sodium humate from sodium aluminate solution by adsorption with alumina dust [J]. The Chinese Journal of Nonferrous Metals, 2017, 27(11): 2356−1362. (in Chinese)

[19] SALIMI R, VAUGHAN J. Crystallisation of tricalcium aluminate from sodium aluminate solution using slaked lime [J]. Powder Technology, 2016, 294: 472−483.

[20] WHITTINGTON B I, FALLOWS T M, WILLING M J. Tricalcium aluminate hexahydrate (TCA) filter aid in the Bayer industry: factors affecting TCA preparation and morphology [J]. International Journal of Mineral Processing, 1997, 49(1): 1−29.

[21] WHITTINGTON B I, CARDILE C M. The chemistry of tricalcium aluminate hexahydrate relating to the Bayer industry [J]. International Journal of Mineral Processing, 1996, 48(1): 21−38.

[22] LITWINEK E, MADEJ D. Structure, microstructure and thermal stability characterizations of C_3AH_6 synthesized from different precursors through hydration [J]. Journal of Thermal Analysis and Calorimetry, 2020, 139(3): 1693−1706.

[23] PAN Xiao-lin, LIU Ji-long, WU Sha-sha, YU Hai-yan. Formation behavior of tricalcium aluminate hexahydrate in synthetic sodium aluminate solution with high alkali concentration and caustic ratio [J]. Hydrometallurgy, 2020, 195: 105373.

[24] PAN Xiao-lin, WU Hong-fei, YU Hai-yan, BI Shi-wen. Precipitation of desilication products in $CaO−Na_2O−Al_2O_3−SiO_2−H_2O$ system based on the Bayer process [J]. Hydrometallurgy, 2020, 197: 105469.

[25] YUAN Jiong-liang, ZHANG Yi. Desiliconization reaction in sodium aluminate solution by adding tricalcium hydroaluminate [J]. Hydrometallurgy, 2009, 95: 166−169.

[26] HONG Tao, LUO Jun, MUMFORD K A, STEVENS, G W, ZHENG Shi-li. Desilication of concentrated alkali solution by novel desilication reagent calcium hydroferrocarbonate: Part III. Standard thermodynamics investigation of desilication reaction using hydroferrite desilication reagents [J]. Hydrometallurgy, 2019, 187: 212−220.

[27] HASHEMI S M, MOHAMEDALI M, SEDGHKERDAR M H, MAHINPEY N. Stability of CaO-based sorbents under realistic calcination conditions: effect of metal oxide supports [J]. ACS Sustainable Chemistry & Engineering, 2022, 10(30): 9760−9769.

[28] LI Xiao-bin, XU Xiang-ming, ZHOU Qiu-sheng, QI Tian-gui, LIU Gui-hua, PENG Zhi-hong, CUI Yuan-fa, LI Jian-pu. Ca_3WO_6 prepared by roasting tungsten-containing materials and its leaching performance [J]. International Journal of Refractory Metals and Hard Materials, 2015, 52: 151−158.

[29] LIU Gui-hua, HUANG Wen-qiang, XIONG Den-fen, WANG Hong-yang, LI Xiao-bin, ZHOU Qiu-sheng, PENG Zhi-hong, QI Tian-gui. Reaction behavior of active phases in aluminum dross [J]. The Chinese Journal of Nonferrous Metals, 2018, 28(11): 2341−2350. (in Chinese)

[30] PATTERSON A L. The Scherrer formula for X-ray particle size determination [J]. Physical Review, 1939, 56(10): 978−982.

[31] TOZAR A, KARAHAN İ H. Structural and corrosion protection properties of electrochemically deposited nano-sized Zn−Ni alloy coatings [J]. Applied Surface Science, 2014, 318: 15−23.

[32] OWENS D K, WENDT R. Estimation of the surface free energy of polymers [J]. Journal of Applied Polymer Science,

1969, 13(8): 1741−1747.
[33] LI Xiao-bin, ZHAO Dong-feng, ZHANG Xuan, LIU Gui-hua, PENG Zhi-hong, ZHOU Qiu-sheng. Effect of surface property of main minerals in red mud on their sedimentation ability [J]. The Chinese Journal of Nonferrous Metals, 2012, 22(1): 281−286. (in Chinese)
[34] LUNER P E, OH E. Characterization of the surface free energy of cellulose ether films [J]. Colloids and Surfaces A: Physicochemical and Engineering Aspects, 2001, 181(1): 31−48.
[35] KWOK D Y, NEUMANN A W. Contact angle measurement and contact angle interpretation [J]. Advances in Colloid and Interface Science, 1999, 81(3): 167−249.
[36] XIN Kun, YAN Kui, GAO Chun, LI Zhen. Carbon storage and its influencing factors in Hainan Dongzhangang mangrove wetlands [J]. Marine and Freshwater Research, 2018, 69(5): 771−779.
[37] WALKLEY A, BLACK I A. An examination of the Degtjareff method for determining soil organic matter, and a proposed modification of the chromic acid titration method [J]. Soil science, 1934, 37(1): 29−38.
[38] CHENG Hong-fei, FROST R L, YANG Jing, LIU Qin-fu, HE Jun-kai. Infrared and infrared emission spectroscopic study of typical Chinese kaolinite and halloysite [J]. Spectrochimica Acta Part A: Molecular and Biomolecular Spectroscopy, 2010, 77(5): 1014−1020.
[39] BUYONDO A K, KASEDDE H, KIRABIRA J B, BONGMIN O. Characterization and treatment effects on Mutaka kaolin for additive in coating: Mineral composition, thermal and structural modifications [J]. Heliyon, 2024, 10(1): e24238.
[40] LI Xiao-bin, WANG Yi-lin, ZHOU Qiu-sheng, QI Tian-gui, LIU Gui-hua, PENG Zhi-hong, WANG Hong-yang. Transformation of hematite in diasporic bauxite during reductive Bayer digestion and recovery of iron [J]. Transactions of Nonferrous Metals Society of China, 2017, 27(12): 2715−2726.
[41] LI Xiao-bin, LI YAN, ZHAO Dong-feng, ZHOU Qiu-sheng, LIU Gui-hua, PENG Zhi-hong, YANG Shuai-shuai, QI Tian-gui. Relationship between $Al(OH)_3$ solubility and particle size in synthetic Bayer liquors [J]. Transactions of Nonferrous Metals Society of China, 2013, 23(5): 1472−1479.
[42] PALMER S J, FROST R L, SMITH M K. Minimising reversion, using seawater and magnesium chloride, caused by the dissolution of tricalcium aluminate hexahydrate [J]. Journal of Colloid and Interface Science, 2011, 353(2): 398−405.
[43] LIU Gui-hua, LI Zheng, QI Tian-gui, ZHOU Qiu-sheng, PENG Zhi-hong, LI Xiao-bin. Continuous changes in electrical conductivity of sodium aluminate solution in seeded precipitation [J]. Transactions of Nonferrous Metals Society of China, 2015, 25(12): 4160−4166.
[44] WU Peng, LIU Gui-hua, LI Xiao-bin, PENG Zhi-hong, ZHOU Qiu-sheng, QI Tian-gui, WANG Yi-lin, SHEN Lei-ting. Removal of organics from Bayer liquors via foam flotation [J]. Journal of Cleaner Production, 2022, 336: 130353.
[45] PYTER R A, ZOGRAFI G, MUKERJEE P. Wetting of solids by surface-active agents: The effects of unequal adsorption to vapor-liquid and solid-liquid interfaces [J]. Journal of Colloid and Interface Science, 1982, 89(1): 144−153.
[46] WINSOR P A. Solvent properties of amphiphilic compounds [M]. Butterworths Scientific Publications, 1954.
[47] CROW D R. Principles and applications of electrochemistry [M]. Routledge, 2017.
[48] NIENHUIS E T, POUVREAU M, GRAHAM T R, PRANGE M P, PAGE K, LORING J S, STACK A G, CLARK A E, SCHENTER G K, ROSSO K M, PEARCE C I, WANG Hsin-wen. Structure and reactivity of sodium aluminate complexes in alkaline solutions [J]. Journal of Molecular Liquids, 2022, 367: 120379.
[49] WU Peng, XUE Teng, LIU Gui-hua, LI Xiao-bin, PENG Zhi-hong, ZHOU Qiu-sheng, QI Tian-gui. Interfacial behavior and micellization of binary surfactant mixtures in the concentrated sodium aluminate solution [J]. Journal of Molecular Liquids, 2021, 334: 116530.
[50] LIU Zi-long, ZHAO Ge, MARK B, LV Qi-chao, SUDHOLTER E J R. Comprehensive review on surfactant adsorption on mineral surfaces in chemical enhanced oil recovery [J]. Advances in Colloid and Interface Science, 2021, 294: 102467.

基于六水铝酸三钙的双电层调控从铝酸钠溶液中短流程脱除有机物

符振江[1]，刘桂华[1]，齐天贵[1]，申雷霆[1]，彭志宏[1]，周秋生[1]，王一霖[1]，房 辉[2]， 王永林[2]

1. 中南大学 冶金与环境学院，长沙 410083；2. 龙口东海氧化铝有限公司，龙口 265713

摘 要：从铝酸钠溶液中经济地脱除有机物是长期以来的研究重点。基于叶滤环节将六水铝酸三钙 (TCA)作为助滤剂的工艺，提出一种短流程同时滤除杂质颗粒和吸附脱除有机物的新方法。在浓缩铝酸钠溶液中制备结晶度低、TCA 含量高、表面能高、晶格畸变大的超细 TCA 样品。同时，TCA 样品在碱性溶液中的 Zeta 电位线性依赖于 TCA 含量，揭示二元混合物 Zeta 电位的可加性。描述在碱性溶液中 TCA 二元混合物双电层的演化规律。此外，超细 TCA 样品对长烷基链及高相对分子质量有机物具有较高的吸附容量，对腐殖酸钠的吸附容量可达 69.69 mg/g(以有机碳计)，而高温溶出过程会显著降低 TCA 的吸附容量。

关键词：有机物脱除；六水铝酸三钙；铝酸钠溶液；Zeta 电位；双电层

(Edited by Bing YANG)